CATALYSIS

Electrically driven proton transfer promotes Brønsted acid catalysis by orders of magnitude

Karl S. Westendorff[1], Max J. Hülsey[2], Thejas S. Wesley[1], Yuriy Román-Leshkov[1,2]*, Yogesh Surendranath[1,2]*

Electric fields play a key role in enzymatic catalysis and can enhance reaction rates by 100,000-fold, but the same rate enhancements have yet to be achieved in thermochemical heterogeneous catalysis. In this work, we probe the influence of catalyst potential and interfacial electric fields on heterogeneous Brønsted acid catalysis. We observed that variations in applied potential of ~380 mV led to a 100,000-fold rate enhancement for 1-methylcyclopentanol dehydration, which was catalyzed by carbon-supported phosphotungstic acid. Mechanistic studies support a model in which the interfacial electrostatic potential drop drives quasi-equilibrated proton transfer to the adsorbed substrate prior to rate-limiting C–O bond cleavage. Large increases in rate with potential were also observed for the same reaction catalyzed by Ti/TiO_yH_x and for the Friedel Crafts acylation of anisole with acetic anhydride by carbon-supported phosphotungstic acid.

Precisely placed charged amino acid residues in enzymatic active sites generate strong, oriented electric fields to promote biological catalysis (*1*–*3*). Similarly, when electrode surfaces are electrically charged, the accumulation of opposing ionic charge in solution generates a sharp electrostatic potential gradient and a correspondingly large oriented electric field at the metal-solution interface (*4*). For electrochemical half-reactions, which involve the net transfer of electrons to or from the electrode, the change in free energy and corresponding rate of the half-reaction is known to be strongly dependent on the electrode potential. Thus, small changes (on the order of 100s of millivolts) in surface electrochemical potential lead to orders of magnitude enhancements in reaction rate (Fig. 1A) (*5*–*11*). This contrasts with redox neutral thermochemical reactions, in which there is no net exchange of electrons to or from the catalytic interface and therefore no change in the reaction's free energy upon varying surface potential. Yet, modulating the interfacial potential has been shown to activate aromatic thiol substrates bound to gold surfaces toward redox neutral hydrolysis, cross-coupling, and amidation reactions (*12*). In contrast to activating a surface-bound substrate, a potentially more general strategy for using interfacial potentials to promote thermochemical reactivity would involve modulating the catalyst directly. However, attempts to use surface potentials to promote thermochemical catalysis by surface-bound active sites have generally observed weak rate-potential scaling, and the mechanisms underlying these relatively modest promotional effects on catalysis remain unclear (Fig. 1B) (*13*–*18*).

For many electrochemical half-reactions, varying the applied potential augments the rate by driving elementary proton-coupled electron transfer (PCET) steps in the reaction sequence (*19*–*21*). We therefore posited that if an elementary PCET step were embedded within an overall thermochemical reaction, the strong potential dependence of the PCET step could be leveraged to promote non-Faradaic thermochemical catalysis. Because interfacial PCET (I-PCET) reactions involve proton exchange across the electric double layer, the foregoing logic suggests that thermochemical reactions catalyzed by proton transfer, namely those subject to Brønsted acid catalysis, could be promoted through the polarization dependence of rate-controlling elementary I-PCET steps (Fig. 1C). Notably, this promotion strategy does not require additional energy input into the system beyond polarizing the catalytic interface, offering a highly energy-efficient approach for accelerating redox-neutral thermochemical reactions.

In this work, we examined the potential dependence of Brønsted acid catalysis. For a model dehydration reaction of 1-methylcyclopentanol with carbon-supported phosphotungstic acid (PTA), we found that interfacial polarization can alter Brønsted acid catalysis turnover frequencies (TOFs) by as much as five orders of magnitude, with potential-dependent scale factors similar to those of electrochemical transformations (10-fold per ~100 mV) despite no change in the net reaction free energy. Mechanistic studies suggest that the strong potential dependence arises from an electrically driven shift in the reaction quotient for a pre-equilibrium proton exchange between PTA and 1-methylcyclopentanol that precedes the rate-determining step (RDS), C–O bond cleavage. Varying the potential serves to alter the catalyst's effective acidity, resulting in an accumulation of protonated alcohol species that react in the rate-limiting step, thereby enhancing the reaction rate. We further found that polarization promotes Brønsted acid catalysis with oxide-coated titanium (Ti) electrodes as well as in a PTA-catalyzed Friedel-Crafts acylation, evincing the generality of this promotion mechanism.

Brønsted acid catalytic activity is strongly dependent on interfacial potential

To investigate the effect of electrochemical potential on Brønsted acid catalysis, we examined the dehydration of 1-methylcyclopentanol in acetonitrile (MeCN) catalyzed by phosphotungstic acid supported on Vulcan carbon (PTA/C). Tetrabutylammonium hexafluorophosphate ([TBA][PF_6]) served as the supporting electrolyte. This probe system was selected specifically to circumvent any convolution with Faradaic reactions, as the tungsten (VI) centers in PTA cannot be further oxidized, the MeCN solvent has a large electrochemical window, and tertiary alcohols are resistant to oxidation at the potentials used in this study (*22*–*24*). We initially focused on an alcohol dehydration because of its relatively simple mechanism compared with that of other Brønsted acid–catalyzed reactions. In this system, all reactions were carried out at 40°C in a solution of 1- or 0.1-M 1-methylcyclopentanol depending on the reaction manifold, with 0.1-M [TBA][PF_6] as the electrolyte and 0.1-M tri-*tert*-butylbenzene as the internal standard. We report all rates versus the decamethylferrocene/decamethylferrocenium redox couple ($DmFc/DmFc^+$) in this solution unless otherwise stated.

We conducted initial experiments in a batch reactor using a colloidal suspension of PTA/C and measured reaction rates by product formation as quantified by nuclear magnetic resonance (NMR) spectroscopy of reaction aliquots. We used 1-M 1-methylcyclopentanol in these initial studies to avoid mass transport limitations in the small, 20- to 30-nm pores of the Vulcan carbon support (supplementary materials, section 3.5). Because not every active site in a PTA/C colloidal suspension can be wired to an external circuit, we conducted these studies by "wirelessly" polarizing the catalyst using redox buffers in solution.

In this polarization method, the reduced and oxidized components of a redox buffer in solution add and remove electrons from the conductive colloidal carbon particles, respectively, to establish electrochemical equilibrium at the carbon-solution interface. This equilibrium sets the electrochemical potential of the carbon particles in a Nernstian fashion based on the standard reduction potential of the redox species and the ratio of its reduced and oxidized components. At higher concentrations of the oxidized species, the electrochemical potential is set positively of the standard reduction potential,

[1]Department of Chemical Engineering, Massachusetts Institute of Technology, Cambridge, MA 02139, USA. [2]Department of Chemistry, Massachusetts Institute of Technology, Cambridge, MA 02139, USA.
*Corresponding author. Email: yroman@mit.edu (Y.R.-L.); yogi@mit.edu (Y.S.)

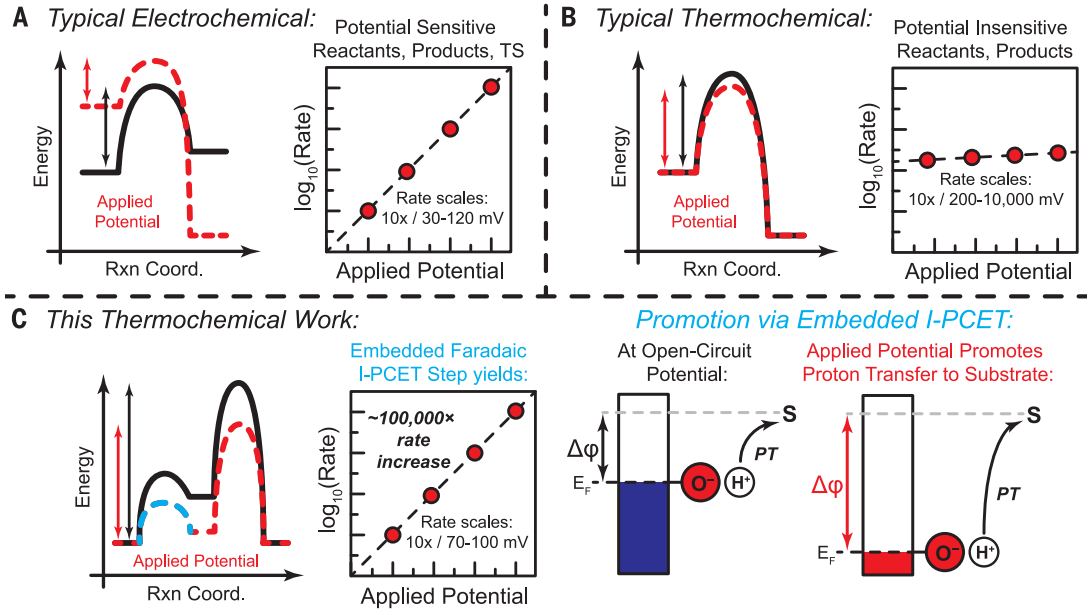

Fig. 1. Similarities and contrasts between typical electrochemical and thermochemical reactions and this work. (**A**) For electrochemical reactions, varying the applied potential alters the overall free energy change for the reaction (left) and can induce large changes in reaction rate (right). (**B**) For thermochemical reactions, varying potential does not change the free energy of reaction (left), and the rate of most thermochemical reactions are weakly dependent on potential (right). (**C**) We show that polarization (Δϕ, the difference in the electrostatic potential between the catalyst and solution) can greatly impact the rate of a thermochemical reaction sequence with an embedded interfacial PCET step (left). The electrostatic potential drop at the surface drives protons to the substrate upon positive polarization, and this driving force increases at increasingly positive potentials (right). Rxn. coord., reaction coordinate; TS, transition state; PT, proton transfer.

whereas at higher concentrations of the reduced species, it is set more negatively. We previously demonstrated the efficacy of this polarization method and use it here to set the potential of the PTA/C catalyst suspension (*25*).

We chose the combination of $[Fe(phen)_3][PF_6]_2$ and $[Fe(phen)_3][PF_6]_3$ as the redox buffer because of its fast outer sphere electron transfer rate (*26*), and because these organometallic complexes are coordinatively saturated, thereby inhibiting covalent binding interactions with the catalytic surface (*26*). Indeed, we found that these redox buffers have negligible catalytic activity on their own, and that varying the overall concentration of the redox buffer does not substantially influence the rate (figs. S9 and S10) of the acid-catalyzed reaction.

We found that catalysis of 1-methylcyclopentanol dehydration at 40°C is strongly dependent on potential in these spontaneous polarization studies. To isolate the PTA turnover frequency (TOF), we measured the reaction rates of the 5% PTA/C powder and subtracted the rates of identically treated Vulcan carbon powder under identical reaction conditions (fig. S11). The background-subtracted rates were divided by the moles of PTA in the catalyst to calculate TOF values, and these values were found to be constant across catalyst loading at a given potential, implying that all PTA sites are similarly active (fig. S12). Using a 15:1 $[Fe(phen)_3][PF_6]_2$:$[Fe(phen)_3][PF_6]_3$ buffer to set the potential of the catalyst to 1150 mV, we measured a TOF of 0.01 s^{-1}. By using a 2:1 $[Fe(phen)_3][PF_6]_2$:$[Fe(phen)_3][PF_6]_3$ redox buffer to raise the potential of the catalyst to 1200 mV, we measured an increased TOF of 0.09 s^{-1}.

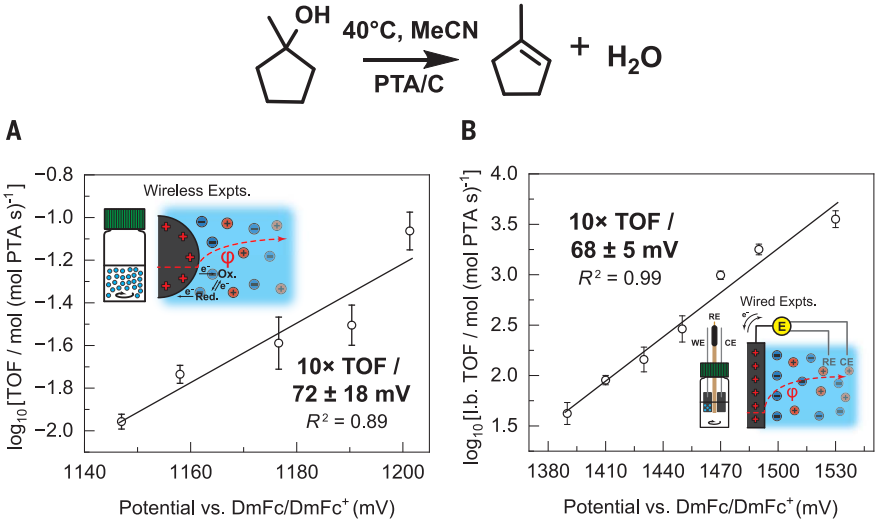

Fig. 2. TOF dependence on applied electrochemical potential for PTA/C catalyzed dehydration of 1-methylcyclopentanol. (**A**) Potential dependence of the TOF of colloidal 5% PTA/C polarized by exposure to varying ratios of $[Fe(phen)_3][PF_6]_2$ and $[Fe(phen)_3][PF_6]_3$. (**B**) Potential dependence of the lower-bound (l.b.) TOF for PTA/C electrodes polarized potentiostatically. All reactions were conducted at 40°C in a solution of either (A) 1-M or (B) 0.1-M 1-methylcyclopentanol in MeCN with 0.1-M $[TBA][PF_6]$ as the electrolyte and 0.1-M tri-*tert*-butylbenzene as the internal standard. Reaction conditions are further detailed in the supplementary materials, sections 3.5 and 4.3. All datapoints shown here are the average of three independent measurements, and the error bars represent the standard deviation of these replicates. The fit to the data was not weighted by the error bars of each point. Expts., experiments; red., reduction; ox., oxidation.

Intermediate buffer ratios were used to set potentials in between these extremes and led to intermediate rates of catalysis. Across five set potentials, we observed a roughly linear trend with a slope corresponding to a scale factor of approximately 10-fold increase in TOF per 72 ± 18–mV increase in potential (Fig. 2A).

To further extend the potential range and explore the extent of the promotion effect, we examined Brønsted acid catalysis with PTA deposited on Sigracet 39 BB carbon paper electrodes. These modified carbon electrodes served as the working electrodes in a conventional undivided three-electrode electrochemical cell, allowing for direct polarization of the

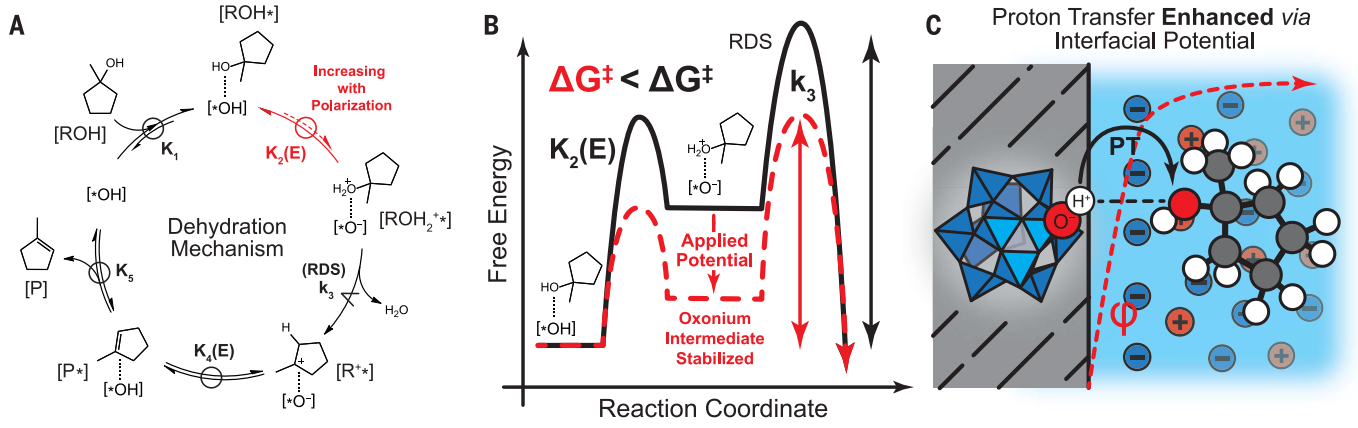

Fig. 3. Schematics of the overall dehydration catalytic cycle, the pre-RDS free energy landscape of the dehydration reaction, and an illustration of the polarized catalytic interface. (**A**) Putative catalytic cycle for PTA/C-catalyzed dehydration of 1-methylcyclopentanol. The key potential-dependent I-PCET step is highlighted in red. (**B**) Free energy landscape diagram of the dehydration reaction (black) that illustrates the effect of shifting the pre-RDS equilibrium on the apparent activation free energy of the reaction with applied potential (red). (**C**) Illustration of the polarized carbon interface with PTA sites donating protons to the substrate. The presence of an interfacial potential drop drives proton transfer, and the proton is invoked to traverse the majority of the potential drop to recover the experimentally measured rate scaling with potential.

interface through a potentiostat (fig. S13). As opposed to Vulcan carbon particles, these monolithic electrodes are nominally nonporous and therefore not subject to internal transport limitations. Consequently, we used 0.1-M 1-methylcyclopentanol in these experiments but maintained otherwise identical reaction conditions to those in the wirelessly polarized experiments. As the reaction was found to be zeroth order in substrate concentration, rates could still be compared across these two conditions. We measured rates by product formation through NMR spectroscopy of reaction aliquots and corrected the raw rates by subtracting the background rate of catalysis by that of the unmodified carbon electrode under identical conditions (fig. S15). These low surface area electrodes prevented accurate quantification of TOF across a wide range of PTA loadings, and thus, we are not certain that every PTA site is equally active in these wired experiments. Therefore, the calculated TOFs should be viewed as lower-bound values. At an applied potential of 1390 mV, we measured a lower-bound TOF of 41 s^{-1}, which increased to 290 s^{-1} at 1450 mV and further increased to 3600 s^{-1} at 1530 mV. Across seven applied potentials, we observed a linear trend with a slope corresponding to an approximate 10-fold increase in lower-bound TOF per 68 ± 5 mV increase in applied potential (Fig. 2B).

The TOF versus potential data for the wired and wireless experiments together indicate that the TOF increases by more than five orders of magnitude over a potential range of 380 mV (Fig. 2). This corresponds to a 10-fold increase in rate per ~70-mV increase in catalyst potential. Immobilization of PTA on carbon is known to attenuate Brønsted acid catalysis rates relative to that of homogeneous PTA (*27*), yet electrical polarization exposes Brønsted acid–catalyzed rates that exceed that of homogeneous PTA (TOF of 5.8 s^{-1}) by several orders of magnitude (*27*). These data indicate that Brønsted acid–catalyzed alcohol dehydration by PTA/C is strongly dependent on the electrochemical potential of the catalyst.

To elucidate the origin of this promotion in reaction rate, we carried out a series of control experiments. For both the wireless and wired experiments, rate data were collected under conditions of differential conversion, and the rate of product formation was found to be constant over time (figs. S16 and S17). This finding precludes convolution from reaching equilibrium conversion and likely precludes substantial active site deactivation or active site generation over the course of our measurements. To assess whether the applied potential altered the bulk reaction medium, we examined the homogeneous catalytic activity after the reaction by reacquiring NMR measurements of reaction aliquots after the PTA/C catalyst was removed from the reaction medium. For the wired experiments, in which the electrode is a small constituent of the reaction medium, we observed no significant changes in product yield over time upon removing the PTA/C electrode (fig. S18). Although we observed a small amount of residual activity after removing the PTA/C powder for the highest potential in the wireless experiments (fig. S19), this contribution is small relative to the overall scaling in rates. These data suggest that neither catalyst leaching nor the generation of a soluble protic species is responsible for the observed scaling of reaction rate with potential. This finding is also consistent with the observed linear reaction profiles (figs. S16 and S17). To examine whether Faradaic pathways significantly contribute to the observed trend in reactivity with potential, we calculated ratios of the measured molar rates of product formation over the steady-state currents for the wired polarization experiments. At 1390 mV, this ratio was >1100, and at 1530 mV, this ratio was >430. Similar ratios were found at intermediate potentials with no clear trend, suggesting that parasitic Faradaic reactions are not responsible for the observed promotion in acid catalysis (fig. S20). To determine whether the observed promotion effect could be ascribed to a permanent change in catalyst structure, we examined the reversibility of the promotion effect by modulating the potential of the working electrode in a single experiment. Switching from 1530 to 1390 mV led to an immediate drop in the lower-bound TOF from 1230 to 8 s^{-1}, and a TOF of 1230 s^{-1} was immediately recovered upon switching back to 1530 mV (fig. S21). These findings suggest that the observed change in catalytic rate cannot be attributed to an irreversible change in the catalyst or support structure. We additionally measured the reaction order with respect to 1-methylcyclopentanol to test whether transport artifacts could convolute the measured rates. For the wirelessly polarized experiments conducted with PTA/C, we found that reaction rates were invariant within error across 1-methylcyclopentanol substrate concentrations from 0.5 to 1 M at both the lowest, 1150 mV, and highest, 1200 mV, potentials set by the redox buffer (figs. S22 and S23). For the wired experiments conducted on nominally nonporous

carbon paper, we found that reaction rates were invariant within error for substrate concentrations beyond 0.1 M at applied potentials of both 1390- and 1470-mV (figs. S24 and S25). Altogether, these results indicate that the reaction is zeroth order in substrate, and that transport artifacts do not substantially convolute our rate measurements in either the wireless or wired experiments.

Next, we conducted a set of experiments to better understand the dehydration reaction mechanism. To examine whether C–O bond cleavage is reversible, we conducted an ^{18}O isotope–tracing experiment by injecting $H_2{}^{18}O$ into the reaction solution and analyzing ^{18}O incorporation in the reactant after measurable conversion (fig. S26). We found no detectable ^{18}O incorporation into 1-methylcyclopentanol through gas chromatography–mass spectrometry (GC-MS) after running the reaction to a conversion comparable to that in our kinetic studies, suggesting that C–O bond cleavage is irreversible in this system (fig. S27) (*28*).

To probe the effect of the interfacial potential drop and corresponding field strength on the reaction, we varied the electrolyte concentration and measured the reaction rate scaling with potential. Whereas we observed a 10x rate enhancement for every 70-mV change in potential in a 0.1-M [TBA][PF_6] electrolyte, the scaling attenuates to 10x every 120 mV in a 0.05-M electrolyte, and we observed no significant scaling with potential in a 0.005-M electrolyte (fig. S28). This trend suggests that the potential-driven kinetic enhancements are sensitive to the gradient in the electrostatic potential profile in the double layer rather than solely the absolute value of the potential at the surface (*4*, *29*). We note that substitution of [TBA][PF_6] with tetrabutyl ammonium bis (trifluoromethanesulfonyl)imide returns the same reaction rate at the highest potential sampled, suggesting that the electrolyte is not directly participating in the reaction other than establishing the double-layer potential profile.

The preceding control experiments and mechanistic studies provided the basis for a mechanistic model for potential-dependent Brønsted acid catalysis depicted in Fig. 3A. Owing to the zeroth order dependence on 1-methylcyclopentanol concentration across the range of catalyst potentials examined here, we infer that the active sites are fully saturated with adsorbed alcohol under all conditions tested (*30*), making the surface-bound alcohol the most abundant surface species. We therefore propose a potential-dependent quasiequilibrated proton transfer from a W–OH moiety to the 1-methylcyclopentanol to generate an oxonium intermediate. To furnish this potential dependence, we assume that the catalyst potential remains constant across this elementary step, as well as across the overall reaction sequence. This constant potential can be ensured either by transient electron flow from the external circuit (for the wired experiments), from the redox buffer (for the wireless experiments), and/or from electron redistribution within the carbon itself to balance the negative surface charge left behind following proton transfer. Irrespective of the mechanism of electron flow, the maintenance of a constant catalyst potential is the reason that this reaction is best viewed as an interfacial proton-coupled electron transfer, rather than simply an interfacial proton transfer that would alter the catalyst potential. This is in line with the understanding of analogous elementary I-PCET steps within net electrochemical half-reactions. Following this I-PCET step, we invoke rate-limiting C–O bond cleavage to release water and generate a tertiary carbocation, which rapidly transfers a proton to the PTA/C active site (with accompanying reverse electron flow), regenerating the catalyst and furnishing the olefin product upon desorption. The rate-limiting C–O cleavage step is supported by the lack of ^{18}O scrambling in the system and agrees with previous literature that found that stepwise, unimolecular elimination mechanisms dominate at solid-liquid interfaces for tertiary alcohols (*31*, *32*).

In this proposed mechanism, the potential-dependence of the dehydration rate arises from shifting the position of the quasiequilibrated I-PCET step [K_2(E) in Fig. 3A] toward product, thereby increasing the population of the pre-RDS oxonium intermediate and lowering the apparent activation free energy of the reaction (Fig. 3B). This can equivalently be interpreted as lowering the "electrochemical" acid dissociation constant (pK_a) of the catalyst by polarizing oxidatively. This electrochemical pK_a is composed of the innate chemical driving force for proton transfer augmented by the electrostatic potential drop at the interface. To derive the rate scaling, we applied the following assumptions: (i) The I-PCET step to form the oxonium intermediate resides in minor equilibrium across the full potential range explored; (ii) proton binding to the PTA can be described by a Langmuirian isotherm; and (iii) the proton traverses the full electrostatic potential drop at the interface in this I-PCET step. With these assumptions, the quasiequilibrium surface population of the oxonium intermediate increases by one decade for every 62-mV increase in applied potential under the reaction conditions (at 40°C), and the scale factor for this I-PCET elementary step is expected to translate fully into the scaling of TOF with potential for the overall reaction (see supplementary materials section 6 for full rate law, potential-dependence derivation, and discussion of potential drop length scale) (*33*–*37*). This predicted scale factor is in close agreement with the observed ~70-mV per decade scale factors (Fig. 2). The change in activation free energy with potential also supports the model presented in Fig. 3B. We measured activation free energies at 1430 and 1490 mV by varying the reaction temperature from 25 to 60°C and found that the activation free energy decreased by 5.3 kJ/mol (fig. S30) (supplementary materials section 6.5), which is in close agreement with the 60-meV or 5.8-kJ/mol change in applied potential.

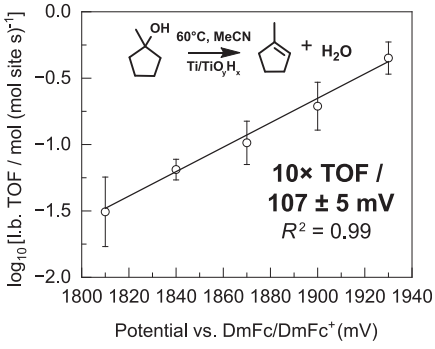

Fig. 4. Potential dependence of Ti foil–catalyzed dehydration of 1-methylcyclopentanol. Lower-bound TOFs for Ti foil–catalyzed 1-methylcyclopentanol dehydration as a function of applied potential. Lower-bound TOF values were calculated assuming that all surface-exposed Ti atoms host active sites. All reactions were run at 60°C in a solution of 0.1-M 1-methylcyclopentanol in MeCN with 0.1-M [TBA][PF_6] as the electrolyte and 0.1-M tri-*tert*-butylbenzene as the internal standard. Reaction conditions are further detailed in the supplementary materials, section 7.1. All datapoints shown here are the average of three independent measurements, and the error bars represent the standard deviation of these replicates. The fit to the data was not weighted by the error bars of each point.

The effect of electrolyte concentration on potential-rate scaling provides additional insight into the mechanism of catalytic promotion. At high electrolyte concentrations (0.1 M), the electrostatic potential drop is sufficiently steep that the adsorbed alcohol experiences a local electrostatic potential comparable to that of bulk solution. Thus, the proton traverses the majority of the interfacial potential drop in the I-PCET step and the corresponding full electron is exchanged with the circuit or redox buffer to hold the potential constant. This leads to the observed high potential-rate scaling in strong electrolytes. By contrast, at low electrolyte concentrations (0.005-M [TBA][PF_6]), the electrostatic potential gradient at the interface is shallower, but the length scale for proton transfer from PTA to the adsorbed substrate remains largely unchanged. Consequently, the proton traverses a smaller fraction of the overall potential drop at reduced electrolyte strengths, and a correspondingly smaller fraction of an electron is exchanged per proton transfer to hold the potential constant. This leads to a dramatic attenuation of

the potential-rate scaling (fig. S31). Notably, this observation argues against a mechanism in which the change in the free energy for proton transfer arises from chemical or inductive effects on the surface-bound species, as previously invoked for polarization-promoted surface reactivity and catalysis (*12*, *14*, *16*). Such effects would alter the innate chemical affinity of the surface site for protons but would be largely insensitive to the electrostatic profile at the interface. As derived in section 6 of the supplementary materials, the observed trend can instead be fully explained by holding the innate chemical affinity of the surface site for protons constant while simply altering the electrostatic potential drop traversed by the proton upon transfer to the substrate. Altogether, these data are consistent with a picture of the polarized catalytic interface depicted in Fig. 3C.

Because the dehydration reaction does not involve net electron exchange (i.e., it is not an electrochemical half reaction), varying the applied potential cannot alter the overall free energy change for dehydration. Consequently, any effect of the applied potential on the forward I-PCET step [K_2(E), Fig. 3A] must be balanced by an opposing effect on the reverse I-PCET step [K_4(E), Fig. 3A] that regenerates the catalyst. Indeed, in our model, any electrons exchanged during the forward I-PCET step are balanced by back electron transfer during the reverse I-PCET step. Consequently, in this model, catalyst regeneration by means of I-PCET from the carbocation to the PTA is expected to be inhibited by ~10-fold for every 62-mV increase in applied potential (at 40°C). However, because this reverse I-PCET is after the RDS, its inhibition with increasing applied potential does not substantially influence the observed kinetics, leading to the observed monotonic increase in reaction rate with positive polarization.

Potential-dependent Brønsted acid catalysis extends to Ti/TiO_yH_x interfaces

The mechanistic model depicted in Fig. 3 implies that promotion of Brønsted acid catalysis by an applied potential should not be limited to a specific material. Indeed, any polarizable interface with surface -OH_x groups should, in principle, function as tunable acid catalysts responsive to interfacial polarization.

To examine this hypothesis, we investigated the same dehydration reaction with polarized Ti foils as working electrodes in a single-cell, three-electrode setup connected to a potentiostat. Because of rapid reaction with O_2, Ti foils invariably contain passivating layers of TiO_2 under reaction conditions (*38*). We envisioned that TiO_yH_x defects in this passivating layer could serve as potential-dependent hosts for Brønsted acid catalysis. Assuming all surface-exposed Ti(IV) ions on a Ti foil electrode host active sites, we found a lower-bound TOF for

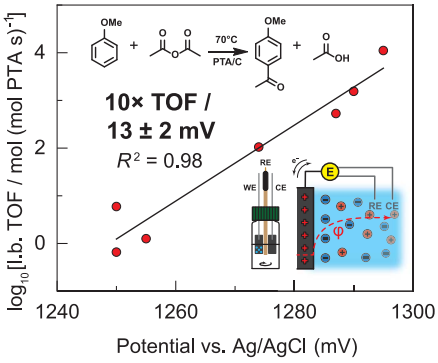

Fig. 5. Potential dependence of PTA/C-catalyzed acylation of anisole. Lower-bound TOFs for PTA/C-catalyzed acylation of anisole with acetic anhydride as a function of applied potential. All reactions were run at 70°C in a solution of 0.84-M acetic anhydride in anisole with 1.2-M [TBA][PF_6] as the electrolyte and the internal standard. Reaction conditions are further detailed in the supplementary materials, section 8.1. All datapoints shown here are individual measurements. WE, working electrode; RE, reference electrode; CE, counter electrode.

1-methylcyclopentanol dehydration of 0.03 s^{-1} at 1810 mV. This lower-bound TOF rose to 0.10 s^{-1} at 1870 mV and to 0.45 s^{-1} at 1930 mV. The data reveal a linear trend with a slope corresponding to 10-fold increase in TOF per 107 ± 5 mV (Fig. 4) increase in applied potential.

We next conducted a series of control experiments, analogous to those for the PTA/C system, to better understand the promotion mechanism for the Ti/TiO_yH_x catalyst. Rate data were collected under conditions of differential conversion, and reaction profiles were again linear over the course of the reaction (fig. S33). This suggests that substantial active site deactivation, active site generation, or approaching equilibrium conversion likely do not significantly contribute to our kinetic measurements. We again found no significant changes in product concentration over time for a given aliquot of reaction solution, suggesting that neither catalyst leaching nor the generation of other soluble protic species contributes to our measured kinetics (fig. S34). We then calculated ratios of measured molar rates over steady-state currents for this system. At 1810 mV, this ratio is >1350, and at 1930 mV, this ratio is >5000. Intermediate potentials return ratios of similar values, indicating that parasitic Faradaic reactions contribute negligibly to the observed reactivity, just as they did for the PTA/C catalyst (fig. S35).

We again examined whether the promotion effect could be ascribed to irreversible catalyst structural changes by modulating the potential back and forth in a single experiment. Switching from 1930 to 1810 mV led to an immediate drop in the lower-bound TOF from 0.33 to 0.003 s^{-1}, and a lower-bound TOF of 0.12 s^{-1} was immediately recovered upon switching back to 1900 mV (fig. S36). As for the PTA/C system, we found that reaction rates were invariant within error across substrate concentrations from 0.1 to 0.5 M, indicating that active sites are saturated with reactant and that transport artifacts do not contribute to the observed kinetics (fig. S37). We further probed for the presence of transport artifacts by rotating cylinder electrode experiments and measured the catalyst TOF as a function of rotation speed. We found the TOF to be independent of rotation speed, indicating that transport artifacts do not contribute substantially to the observed kinetics (fig. S41). This corroborates the zeroth-order dependence on reactant concentration for this system. Together, these findings suggest a mechanistic model for this Ti/TiO_yH_x catalyst similar to that of the PTA/C catalyst.

Notably, the above mechanism predicts that the reaction rate will become independent of applied potential at sufficiently high potentials that drive the I-PCET step to major equilibrium [K_2(E) > 1 (Fig. 3B)]. Under these conditions, the oxonium intermediate becomes the most abundant surface species, and the rate of the reaction is governed purely by the potential-independent rate of C–O bond cleavage (fig. S40). This translates to a potential-independent plateau in the TOF. This plateau region was inaccessible for PTA/C because of substantial parasitic background current beyond 1530 mV but was observed for the more inert Ti/TiO_yH_x at potentials beyond 1960 mV, with the lower-bound TOF remaining at ~0.76 s^{-1}, invariant with potential up to 2310 mV (fig. S43). The reaction is still zeroth order in substrate in this potential-independent regime, and so the observed potential-independence does not arise from transport artifacts. This observation of a potential-independent regime further supports the preequilibrium I-PCET mechanistic model put forward in Fig. 2.

Comparable TOFs of the PTA/C and Ti/TiO_yH_x electrodes were achieved at substantially different potentials. Although the lower-bound TOFs for the Ti/TiO_yH_x system may be gross underestimates, this factor alone is insufficient to explain the 630-mV potential offset in TOFs between the two catalysts. We speculate that differences in the onset potential of reactivity stem at least partially from the innate acidity of these materials. Because TiO_yH_x is an intrinsically weaker acid than PTA, the former requires a greater applied potential to lower its electrochemical pK_a to a level sufficient to spur Brønsted acid catalysis at measurable rates (*39*, *40*). We further speculate that the slightly higher scale factor, 107 ± 5 versus 68 ± 5 mV per decade, may arise from a small potential drop through the dielectric titanium oxide layer that separates the metallic Ti from the surface-exposed TiO_yH_x active sites (*41*). Overall, these data point to the generality of the observed Brønsted acid catalysis promotion effect by

means of interfacial electrical polarization and suggest that a wide variety of catalysts may be promoted through this methodology.

The promotion effect extends to a Brønsted acid–catalyzed acylation reaction.

To further explore the generality of interfacial electric field promotion, we examined a completely different Brønsted acid–catalyzed reaction class, a Friedel Crafts acylation, which results in net C–C bond formation rather than dehydration. Specifically, we investigated the acylation of anisole with acetic anhydride to produce para-methoxyacetophenone and acetic acid. Akin to the dehydration reaction system described previously, the overall reaction cannot reasonably be broken down into Faradaic half-reactions.

For this acylation reaction, we conducted wired polarization experiments analogous to those for the 1-methylcyclopentanol dehydration reaction. We again used PTA drop cast onto carbon paper as a working electrode and varied its potential in the same cell configuration as the dehydration systems. We again measured the rate of product formation with NMR spectroscopy of reaction aliquots (figs. S44 and S45). The reaction was run at 70°C in a solution of a 9:1 molar ratio of anisole to acetic anhydride with 1.2-M [TBA][PF_6] as the electrolyte. In these reactions, anisole is both a reactant and the solvent.

As for the dehydration reaction, we found that this acylation reaction is also strongly potential dependent. The TOF for PTA/C-catalyzed acylation increased from 0.66 s^{-1} at 1250 mV versus Ag/AgCl to 11,000 s^{-1} at 1295 mV (Fig. 5). We observed no background activity from the carbon paper support. The TOF versus potential data produce a trendline where the TOF increases approximately four orders of magnitude over a potential range of 45 mV, thereby representing a scale factor of a 10-fold change in TOF for every ~13 ± 2 mV of applied potential.

We performed control experiments analogous to those for the PTA/C and Ti/TiO_yH_x dehydration systems to better understand the potential dependence observed in this system. To minimize contributions from changes in reaction concentrations, we collected rate data at differential conversion. As for the dehydration reactions, we again observed reaction profiles that were linear over the course of the reaction, suggesting that changes in active site identity, quantity, or activity are likely negligible in our system over the timescale of the reaction (fig. S46). To quantify any contributions to catalysis from the reaction solution, we measured the concentration of products over time in a reaction aliquot that was no longer in contact with the polarized interface (fig. S47). We found no significant change in the amount of product over time, suggesting that catalysis is confined entirely to the electrode interface. To determine whether the observed potential dependence was Faradaic in nature, we calculated ratios of molar rates to the steady-state current. At the lower potentials tested (~1250 mV versus Ag/AgCl), these ratios were 0.05 to 0.2, but quickly rise to >2.5 at 1275 mV and to 8.5 at 1295 mV (fig. S48). This more complex medium contains species known to undergo oxidative decomposition by means of, for example, Kolbe oxidation of acetic acid, contributing to much higher parasitic Faradaic currents. Irrespective of the source of the parasitic Faradaic current, the large changes in the above ratios across the potential range suggest that Faradaic processes are not the cause of the observed promotion. We ascribe the large changes in these ratios to the much stronger potential dependence of the Brønsted acid catalysis promotion relative to parasitic background Faradaic processes.

This finding suggests that potential-dependent Brønsted acid catalysis can be applied across a variety of reactions. Although the scale factor of 13 mV per decade in rate is extremely steep and measured over a small potential window, this observation nonetheless emphasizes the importance of measuring and controlling catalyst potential. Although a detailed mechanistic model for this potential dependence is not yet in hand, we speculate that the strong potential dependence may arise from a combination of multiple rate-controlling I-PCET steps and/or cooperative non-Langmuirian adsorption isotherms in this exotic reaction medium.

Conclusions

This work highlights the powerful influence that interfacial potential has on the activities of Brønsted acid catalysts. Although more studies are needed to determine which reactions are most sensitive to interfacial potential and the precise associated underlying mechanistic bases, these findings establish that dramatic changes in rate can be obtained by altering the driving force for interfacial proton transfer steps embedded within an overall non-Faradaic reaction. Our data suggest that this promotion results from a change in the electrostatic potential difference between the catalyst active sites and the substrate rather than a direct change in the innate chemical affinity of the active site itself. Thus, this promotion strategy can be used in combination with classical strategies for tuning catalytic activity (e.g., alloying) that aim to modulate the innate binding affinities of surface active sites to key catalytic intermediates.

In this study, we polarized the catalyst through electron flow to an external circuit or redox buffer. However, interfacial polarization can also be imposed through charge transfer between a catalyst and a support and/or promoter. Thus, our findings suggest that promoter and support effects on catalysis may arise, in part, from modulation of the catalyst potential. Methods for quantifying catalyst potentials across diverse supports and in the presence of varying promoters should enable a deeper understanding of the role of interfacial polarization in these classical promotion strategies (*42*). Altogether, these results indicate that the interfacial potential may play a critical role in heterogeneous Brønsted acid–catalyzed reactions, and we posit that other thermochemical reaction classes may also be substantially influenced by this previously underappreciated reaction parameter.

REFERENCES AND NOTES

1. S. D. Fried, S. Bagchi, S. G. Boxer, *Science* **346**, 1510–1514 (2014).
2. C. Zheng *et al*., *Nat. Chem.* **14**, 891–897 (2022).
3. N. G. Léonard, R. Dhaoui, T. Chantarojsiri, J. Y. Yang, *ACS Catal.* **11**, 10923–10932 (2021).
4. John O'M. Bockris, Amulya K.N. Reddy, Maria Gamboa-Aldeco, *Modern Electrochemistry 2A: Fundamentals of Electrodics* (Springer, ed. 2, 2001).
5. J. Wang, F. Xu, H. Jin, Y. Chen, Y. Wang, *Adv. Mater.* **29**, 1605838 (2017).
6. S. Díaz-Coello, G. García, M. C. Arévalo, E. Pastor, *Int. J. Hydrogen Energy* **44**, 12576–12582 (2019).
7. J. X. Wang, F. A. Uribe, T. E. Springer, J. Zhang, R. R. Adzic, *Faraday Discuss.* **140**, 347–362, discussion 417–437 (2008).
8. J. Ge, O. B. Isgor, *Mater. Corros.* **58**, 573–582 (2007).
9. K. Kanno, M. Suzuki, Y. Sato, *Corros. Sci.* **20**, 1059–1066 (1980).
10. J. Zhang *et al*., *ACS Catal.* **10**, 8597–8610 (2020).
11. S. Z. Oener, M. J. Foster, S. W. Boettcher, *Science* **369**, 1099–1103 (2020).
12. J. Heo *et al*., *Science* **370**, 214–219 (2020).
13. C. G. Vayenas, I. V. Yentekakis, S. I. Bebelis, S. G. Neophytides, *Phys. Chem. Chem. Phys.* **99**, 1393–1401 (1995).
14. P. Vernoux *et al*., *Chem. Rev.* **113**, 8192–8260 (2013).
15. A. A. Khechfe *et al*., *ACS Catal.* **12**, 906–912 (2022).
16. C. G. Vayenas, S. Bebelis, C. Pliangos, S. Brosda, D. Tsiplakides, *Electrochemical Activation of Catalysis: Promotion, Electrochemical Promotion, and Metal-Support Interactions* (Kluwer Academic Publishers, 2001).
17. T. M. Onn *et al*., *J. Am. Chem. Soc.* **144**, 22113–22127 (2022).
18. C. F. Gorin, E. S. Beh, M. W. Kanan, *J. Am. Chem. Soc.* **134**, 186–189 (2012).
19. J. M. Savéant, *Energy Environ. Sci.* **5**, 7718–7731 (2012).
20. J. M. Mayer, *Annu. Rev. Phys. Chem.* **55**, 363–390 (2004).
21. J. N. Schrauben *et al*., *Science* **336**, 1298–1301 (2012).
22. J. F. Keggin, *Nature* **131**, 908–909 (1933).
23. H. Lund, O. Hammerich, M. Dekker, *Organic Electrochemistry* (Wiley & Sons, 2001).
24. D. T. Sawyer, A. Sobkowiak, J. L. Roberts, *Electrochemistry for Chemists* (, 1995).
25. T. S. Wesley, Y. Román-Leshkov, Y. Surendranath, *ACS Cent. Sci.* **7**, 1045–1055 (2021).
26. M. D. Luque de Castro, M. Valcarcel, F. N. Albahadily, H. A. Mottola, *J. Electroanal. Chem. Interfacial Electrochem.* **219**, 139–151 (1987).
27. F. Lefebvre, P. Dupont, A. Auroux, *React. Kinet. Catal. Lett.* **55**, 3–9 (1995).
28. C. J. Hastings, R. G. Bergman, K. N. Raymond, *Chemistry* **20**, 3966–3973 (2014).
29. W. Schmickler, E. Santos, *Interfacial Electrochemistry* (Springer-Verlag, ed. 2, 2010).
30. I. Chorkendorff, J. W. Niemantsverdriet, *Concepts of Modern Catalysis and Kinetics* (Wiley, ed. 3, 2017).
31. B. C. Gates, J. S. Wisnouskas, H. W. Heath, *J. Catal.* **24**, 320–327 (1972).
32. H. Grisebach, J. B. Moffat, *J. Catal.* **80**, 350–357 (1983).
33. M. N. Jackson, M. L. Pegis, Y. Surendranath, *ACS Cent. Sci.* **5**, 831–841 (2019).

34. R. E. Warburton *et al*., *J. Am. Chem. Soc.* **142**, 20855–20864 (2020).
35. J. M. Mayer, *J. Am. Chem. Soc.* **145**, 7050–7064 (2023).
36. M. F. Delley, E. M. Nichols, J. M. Mayer, *J. Am. Chem. Soc.* **143**, 10778–10792 (2021).
37. M. F. Delley, E. M. Nichols, J. M. Mayer, *J. Phys. Chem. C Nanomater. Interfaces* **126**, 8477–8488 (2022).
38. L. I. Vergara, M. C. G. Passeggi Jr., J. Ferrón, *Appl. Surf. Sci.* **187**, 199–206 (2002).
39. A. E. A. A. Said, M. M. M. Abd El-Wahab, M. M. Abdelhak, *React. Kinet. Mech. Catal.* **122**, 433–449 (2017).
40. A. Gervasini, A. Auroux, *J. Catal.* **131**, 190–198 (1991).
41. R. A. Parker, *Phys. Rev.* **124**, 1719–1722 (1961).
42. T. S. Wesley *et al*., *Chem. Sci.* **14**, 7154–7160 (2023).

ACKNOWLEDGMENTS

The authors thank the entirety of the Surendranath and Román labs for their support and feedback throughout this project. We especially thank C. Costentin, N. Razdan, H.-X. Wang, J. Kephart, R. Zhu, J. Watson, M. Dakhchoune, M. Webber, K. Lodaya, V. Mannava, X. Wang, M. Manetsch, K. Groenhout, and M. Farpón for their valuable feedback on the manuscript. We thank K. McCormick and A. Brenner for their assistance during inductively coupled plasma–MS and GC-MS measurements, respectively. We thank G. Drake, B. Dinakar, and B. Johnson for their assistance in transport phenomenon discussions. We thank Y. Zhang for assistance during scanning transmission electron microscopy and energy-dispersive x-ray spectroscopy measurements; M. Kumar for assistance during electrospray ionization–MS measurements; and W. Massefski, B. Adams, and S. Willis for assistance during NMR measurements. **Funding:** Y.S. acknowledges support from the Air Force Office of Scientific Research under award no. FA9550-20-1-0291, and Y.R.-L. acknowledges support from the US Department of Energy, Office of Basic Energy Sciences, under award no. DE-SC0016214. K.S.W. and T.S.W. acknowledge support from the National Science Foundation Graduate Research Fellowship under grant no. 174530, and M.J.H. acknowledges support from Schmidt Futures for a postdoctoral fellowship. **Author contributions:** Conceptualization: K.S.W., Y.R.-L., and Y.S.; Data curation: K.S.W.; Formal analysis: K.S.W. and M.J.H.; Funding Acquisition: Y.R.-L. and Y.S.; Investigation: K.S.W., M.J.H., and T.S.W.; Methodology: K.S.W.; Project administration: Y.R.-L. and Y.S.; Resources: Y.R.-L. and Y.S.; Supervision: Y.R.-L. and Y.S.; Validation: K.S.W. and M.J.H.; Visualization: K.S.W.; Writing – original draft: K.S.W. and Y.S.; Writing – review and editing: K.S.W., M.J.H., T.S.W., Y.R.-L., and Y.S. **Competing interests:** K.S.W., M.J.H., T.S.W., Y.R.-L., and Y.S. are inventors on patent application #63/513,371, submitted by the Massachusetts Institute of Technology, that covers the use of polarized interfaces to generate Brønsted acid catalysts. **Data and materials availability:** All data are available in the main text or the supplementary materials.

SUPPLEMENTARY MATERIAL

science.org/doi/10.1126/science.adk4902
Materials and Methods
Supplementary Text
Figs. S1 to S48
References (*43*–*47*)

Submitted 24 August 2023; accepted 11 January 2024
10.1126/science.adk4902